

Spin-phonon interactions and magnetoelectric coupling in $\text{Co}_4\text{B}_2\text{O}_9$ ($B = \text{Nb}, \text{Ta}$)

K. Park,¹ J. Kim,² S. Choi,^{2,3,4} S. Fan,¹ C. Kim,⁵ D. G. Oh,⁶ N. Lee,⁶ S. -W. Cheong,^{2,7} V. Kiryukhin,² Y. J. Choi,⁶ D. Vanderbilt,² J. H. Lee,⁵ and J. L. Musfeldt^{1,8}

¹*Department of Chemistry, University of Tennessee, Knoxville, Tennessee 37996, USA*

²*Department of Physics and Astronomy, Rutgers University, Piscataway, New Jersey 08854, USA*

³*Center for Integrated Nanostructure Physics, Institute for Basic Science, Suwon 16419, Republic of Korea*

⁴*Sungkyunkwan University, Suwon 16419, Republic of Korea*

⁵*Department of Energy and Chemical Engineering, Ulsan National Institute of Science and Technology (UNIST), Ulsan, Korea*

⁶*Department of Physics, Yonsei University, Seoul 03722, Korea*

⁷*Rutgers Center for Emergent Materials, Rutgers University, Piscataway, New Jersey 08854 USA*

⁸*Department of Physics and Astronomy, University of Tennessee, Knoxville, Tennessee 37996, USA*

(*Electronic mail: musfeldt@utk.edu)

(Dated: 12 April 2023)

In order to explore the consequences of spin-orbit coupling on spin-phonon interactions in a set of chemically-similar mixed metal oxides, we measured the infrared vibrational properties of $\text{Co}_4\text{B}_2\text{O}_9$ ($B = \text{Nb}, \text{Ta}$) as a function of temperature and compared our findings with lattice dynamics calculations and several different models of spin-phonon coupling. Frequency vs. temperature trends for the Co^{2+} shearing mode near 150 cm^{-1} reveal significant shifts across the magnetic ordering temperature that are especially large in relative terms. Bringing these results together and accounting for noncollinearity, we obtain spin-phonon coupling constants of -3.4 and -4.3 cm^{-1} for $\text{Co}_4\text{Nb}_2\text{O}_9$ and the Ta analog, respectively. Analysis reveals that these coupling constants derive from interlayer (rather than intralayer) exchange interactions and that the interlayer interactions contain competing antiferromagnetic and ferromagnetic contributions. At the same time, beyond-Heisenberg terms are minimized due to fortuitous symmetry considerations, different than most other $4d$ - and $5d$ -containing oxides. Comparison with other contemporary oxides shows that spin-phonon coupling in this family of materials is among the strongest ever reported, suggesting an origin for magnetoelectric coupling.

Magnetic materials hosting both transition metal centers and heavy elements are contemporary platforms for the study of chemical bonding and novel properties. The strategy is that $3d$ ions deliver localized orbitals, high spin, and strong electron correlation, whereas $4d$ and $5d$ centers contribute more diffuse orbitals, greater hybridization, a tendency toward dimerization, and spin-orbit coupling that competes on an equal footing with electron correlations.¹⁻⁴ This competition endows these materials with remarkable properties including ultra-hard magnetism,^{5,6} two-sublattice magnetism with frustration⁷⁻⁹ or independent ground states,^{10,11} and mixing across broad energy scales.¹² One important consequence of spin-orbit interactions in these systems is spin-phonon coupling, conventionally described in terms of how the exchange interactions are modulated by particular displacement patterns.^{6-9,13-16} In addition to revealing how materials communicate across different energy scales, these interactions can drive multiferroicity.¹⁷⁻¹⁹

The $\text{Co}_4\text{B}_2\text{O}_9$ ($B = \text{Nb}, \text{Ta}$) system is quasi-two-dimensional mixed metal oxide with a $P\bar{3}c1$ space group [Fig. 1].²⁰ This corundum-type structure is derived from Cr_2O_3 such that four Cr sites are occupied by the mag-

netic Co^{2+} ions and two nonmagnetic Nb^{5+} or Ta^{5+} ions reside on the B sites. The octahedrally-coordinated Co^{2+} centers are trigonally distorted and both edge- and face-sharing. The B ions are arranged into vertical columns and occupy trigonally distorted octahedral sites in the buckled layer. Both systems order antiferromagnetically at $T_N = 27$ and 20 K for $\text{Co}_4\text{Nb}_2\text{O}_9$ and the Ta analog, respectively.^{21,22} Originally thought to host collinear ab -plane spin structure with a small moment along c ,^{20,23} recent work establishes a noncollinear spin arrangement - with a different magnetic space group.²⁴⁻²⁶ A number of teams report magnetostriction across T_N .²⁷⁻²⁹ Under magnetic field, these materials reveal a spin-flop transition (at 0.3 T for $H \parallel ab$),^{21,22,27} large magnetoelectric coupling,^{27,28,30-32} magnetodielectric behavior,^{32,33} a symmetry reduction with asymmetric distortion,²⁹ and spin excitations with magnetoelectric characteristics.³⁴ The magnetoelectric coupling is approximately $\alpha_{[110]} = 20 \text{ ps/m}$ for both compounds.^{27,28,30,31} The interaction is nonlinear,^{35,36} and a polarization memory effect is observed in the paramagnetic phase.³⁷ Despite evidence for magnetostriction across T_N ,^{23,28,29,38} and proposals that cast spin-phonon coupling as the underlying mechanistic driver for these effects,^{24,27,30,38,39} the fundamental

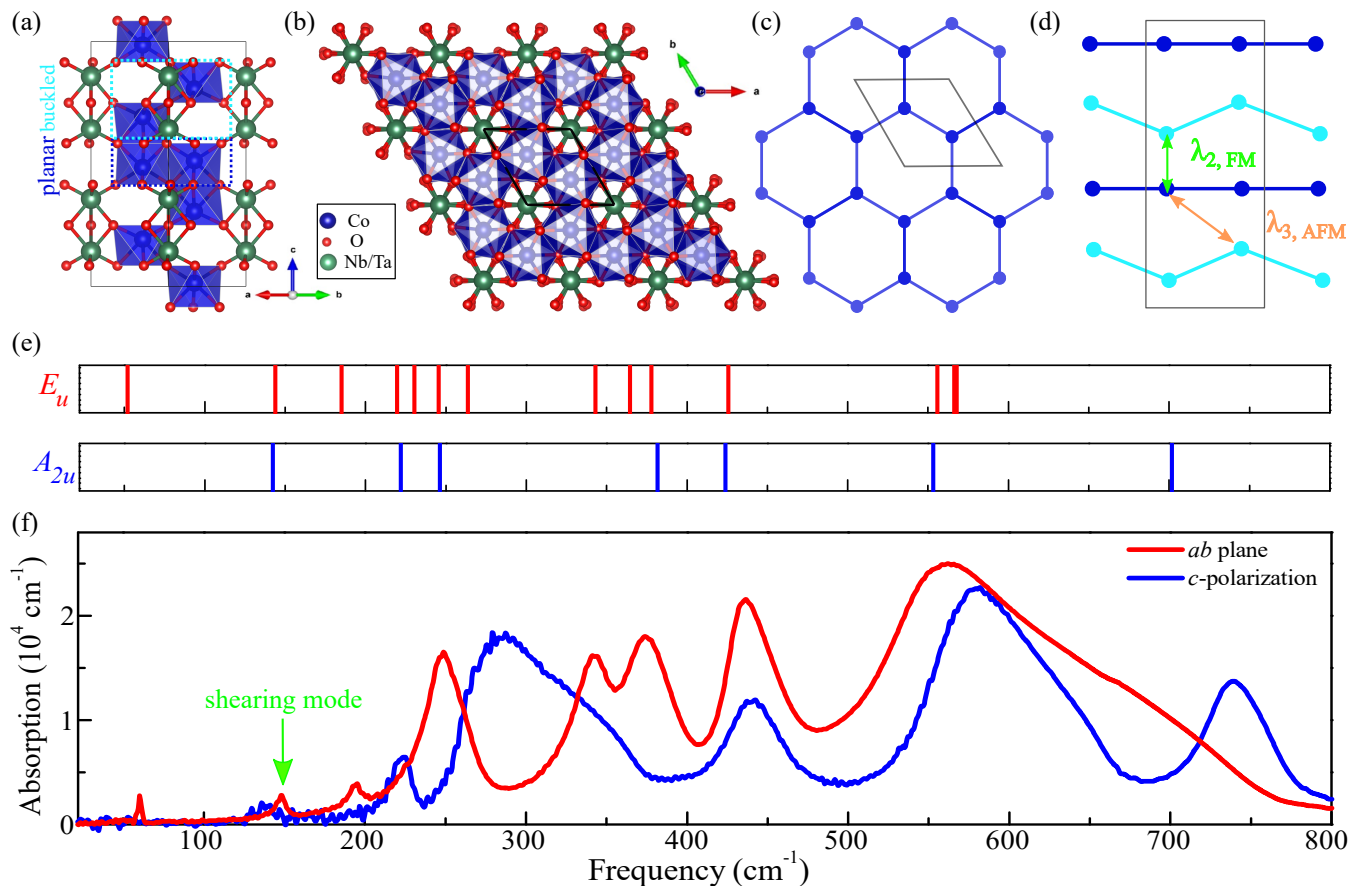


FIG. 1. (a, b) Crystal structure of $\text{Co}_4\text{Nb}_2\text{O}_9$.^{22,26,36} Blue, red, and green represent Co, O, and Nb/Ta centers. Octahedra are drawn only for magnetic ions. (c) A simplified view of the planar Co^{2+} layer shows a honeycomb-like structure. (d) Schematic illustrating the planar and buckled layers. Only Co^{2+} ions are shown. There are two relevant interlayer interactions ($\lambda_{2,FM}$ and $\lambda_{3,AFM}$). (e) Calculated E_u and A_{2u} phonon frequencies. (f) Polarized infrared absorption of $\text{Co}_4\text{Nb}_2\text{O}_9$ at 300 K. The response of $\text{Co}_4\text{Ta}_2\text{O}_9$ is similar and shown in Fig. S1 of the Supplementary information.

excitations of the lattice and their changes across the magnetic ordering transitions are under-explored with only one Raman study of polycrystalline sample identifying modest coupling in two low-frequency modes.³³ $\text{Co}_4\text{Nb}_2\text{O}_9$ and the Ta analog are also ideal platforms for unraveling structure-property relations - not just across simple trends but in higher level coupling processes as well.⁴⁰

In order to explore these issues in greater depth, we combine polarized infrared reflectance, a symmetry analysis, and lattice dynamics calculations to reveal the vibrational properties of $\text{Co}_4\text{Nb}_2\text{O}_9$ and $\text{Co}_4\text{Ta}_2\text{O}_9$ across their magnetic ordering transitions. We find that the in-plane Co-containing shearing mode couples strongly to the spin system, red-shifting across T_N in both materials. The frequency shifts are extremely large, leading to coupling constants of -3.4 and -4.3 cm^{-1} in $\text{Co}_4\text{Nb}_2\text{O}_9$ and the Ta analog, respectively. Remarkably, analysis of the spin-phonon coupling demonstrates that this displacement pattern modulates only the inter-plane magnetic interactions and that the latter contains competing antiferromagnetic and ferromagnetic terms. In addi-

tion to comparisons with other contemporary oxides, we discuss how unique inter-layer spin-phonon interactions drive magnetoelectric coupling in this class of materials.

High-quality single crystals of $\text{Co}_4\text{Nb}_2\text{O}_9$ and $\text{Co}_4\text{Ta}_2\text{O}_9$ were grown by flux techniques.^{26,36} Near normal reflectance was measured over a wide frequency range ($25 - 55,000$ cm^{-1}) using a series of spectrometers including a Bruker 113v Fourier transform infrared spectrometer equipped with a liquid helium cooled bolometer detector, a Bruker Equinox 55 equipped with an infrared microscope, and a Perkin-Elmer Lambda-1050 grating spectrometer. Appropriate polarizers revealed the ab -plane and c -axes response. A Kramers-Kronig analysis was used to obtain the optical constants.⁴¹ We employed a constant low frequency extrapolation and a high frequency extrapolation of $\omega^{-1.75}$. The infrared absorption, $\alpha(\omega)$, and the real part of the optical conductivity, $\sigma_1(\omega)$, are of primary interest in this work. Open-flow cryostats provided temperature control. The theoretical phonon frequencies were calculated using the VASP code.^{42,43} The pseudopotentials are of the projector-augmented-wave type as implemented

in VASP,^{44,45} with valence configurations $3d^7 4s^2$ for Co, $2s^2 sp^4$ for O, $4d^3 4p^6 5s^2$ for Nb, and $5d^3 6s^2$ for Ta. The exchange-correlation functional is described by the Perdew-Burke-Ernzerhof type generalized gradient approximation,⁴⁶ with Dudarev type Hubbard U correction⁴⁷ on Co $3d$ orbits by 3 eV. The plane-wave cut-off energy is set to 400 eV. The Brillouin zone sampling grid is $12 \times 12 \times 4$ including the Γ point. Spin-orbit coupling is not taken into account. The structural coordinates are relaxed within a force threshold of 1.0 meV/Å. To obtain the Γ point phonon frequencies, the dynamical matrix is calculated with the primitive hexagonal cell by using density-functional-perturbation theory⁴⁸ and is processed with the PHONOPY code.⁴⁹ The oscillator strength and dielectric function are calculated by combining Born effective charge tensors and high frequency dielectric constant from the electron response.^{50,51}

Figure 1(e, f) summarizes the infrared response of $\text{Co}_4\text{Nb}_2\text{O}_9$. A symmetry analysis reveals $7A_{2u} + 14E_u$ infrared-active modes and $7A_{1g} + 15E_g$ Raman-active modes. The doubly-degenerate E_u vibrational modes appear in the ab -plane whereas the singly-degenerate A_{2u} modes vibrate along c . The Ta analog is isostructural with a $P\bar{3}c1$ space group and D_{3d} point group symmetry. As a result, the spectrum of $\text{Co}_4\text{Ta}_2\text{O}_9$ is quite similar to that of the Nb-containing compound [Fig. S1, Supplementary information]. Overall, the number of infrared-active modes and their peak positions are nearly identical in both $\text{Co}_4\text{Nb}_2\text{O}_9$ and $\text{Co}_4\text{Ta}_2\text{O}_9$. A summary and detailed comparison between the experimental and theoretical phonon frequencies, symmetries, and displacement patterns is available in Table S6, Supplementary information. The modes related to the heavy Nb and Ta centers appear at the lowest frequencies since $\omega \sim \sqrt{k/\mu}$. We also expect features involving Nb to vibrate at slightly higher frequencies than those involving Ta due to simple mass effects. Here, ω is the frequency, k is the spring constant, and μ is the effective mass. We can test this supposition by examining the mode displacement patterns and realizing that the E_u modes at $60(58) \text{ cm}^{-1}$ and the A_{2u} modes at $138(128) \text{ cm}^{-1}$ reflect the presence of Nb vs. Ta, respectively. The E_u symmetry phonon near 150 cm^{-1} that involves shearing of the Co planes against each other will be important in our discussion as well. This structure is marked with a green arrow in Fig. 1(f). We also studied the temperature dependence of the phonons in $\text{Co}_4\text{Nb}_2\text{O}_9$ and the Ta analog. The majority of features move systematically with decreasing temperature. The E_u symmetry shearing mode near 150 cm^{-1} is the only exception.

Figure 2(a, c) displays a close-up view of the E_u symmetry vibrational mode near 150 cm^{-1} in both materials. This feature hardens with decreasing temperature in the paramagnetic phase and softens across T_N in both systems. It is the only mode that displays this behavior. The Nb compound hosts a sharp frequency shift across the magnetic ordering temperature whereas the Ta ana-

log reveals a gradual transition with a sluggish frequency shift and noticeable precursor effect. As shown in Fig. 2(b, d), we fit frequency vs. temperature trends in the paramagnetic phase using a Boltzmann sigmoidal model to capture anharmonic effects:

$$\omega(T) = \frac{(\omega_o - \omega_h)}{(1 + e^{((T-T_i)/dT)})} + \omega_h. \quad (1)$$

Here, ω_h and ω_o are the high and low temperature limits; T_i and dT are the inflection point and the width of the distribution. As demonstrated by the deviation from the anharmonic phonon model fit below the magnetic ordering transition, this phonon engages in strong spin-phonon coupling in both $\text{Co}_4\text{Nb}_2\text{O}_9$ and $\text{Co}_4\text{Ta}_2\text{O}_9$.^{6,52,53} We also employed line width effects to extract phonon lifetimes. Focusing on the Co^{2+} layer shearing mode, we find phonon lifetimes of 0.75 and 0.6 ps at room temperature in $\text{Co}_4\text{Nb}_2\text{O}_9$ and the Ta analog, respectively. They drop slightly with decreasing temperature and rise sharply below T_N . The latter is consistent with fewer scattering events due to spin ordering.^{54,55} Details are available in the Supplementary information.

In magnetic materials, it is well-known that phonon frequencies can be sensitive to the development of near-neighbor spin correlations.^{15,16,56,57} In such cases, the frequency is expressed as:⁵⁸

$$\omega = \omega_o + \lambda \langle S_i \cdot S_j \rangle. \quad (2)$$

Here, ω_o is the unperturbed phonon frequency that is nicely revealed from the fit in Fig. 2(b, d) at base temperature, ω is the renormalized phonon frequency due to spin-phonon interactions, $\langle S_i \cdot S_j \rangle$ is the spin-spin correlation function, and λ is the spin-phonon coupling constant. Using Eqn. 2, our frequency vs. temperature trends, and the model fits of $\omega(T)$ shown in Fig. 2(b, d), we extract frequency shifts across the magnetic ordering transitions and calculate spin-phonon coupling constants for $\text{Co}_4\text{Nb}_2\text{O}_9$ and $\text{Co}_4\text{Ta}_2\text{O}_9$.

The displacement pattern of the participating phonon is also key to our analysis. As a reminder, our calculations predict that the 150 cm^{-1} phonon mode is an out-of-phase E_u symmetry displacement involving the Co centers in which the planar and buckled layers vibrate against each other. The Nb and Ta centers do not participate very much in the motion. As a result, the relevant motion contains only one spin-containing center: Co^{2+} with $S = \frac{3}{2}$. With this insight and the fact that $\langle S_i \cdot S_j \rangle$ goes as S^2 in the low-temperature limit, we see that the spin-spin correlation function can be approximated as $\langle S_i \cdot S_j \rangle \sim S^2 = (\frac{3}{2})^2 = \frac{9}{4}$. $\text{Co}_4\text{Nb}_2\text{O}_9$ has a frequency shift ($\Delta\omega$) across T_N of -7.5 cm^{-1} . In other words, the mode softens across the magnetic ordering temperature. This means that the bond between layers gets weaker due to magnetism. We extract a spin-phonon coupling constant (λ) of -3.3 cm^{-1} . $\text{Co}_4\text{Ta}_2\text{O}_9$ has a larger frequency shift than $\text{Co}_4\text{Nb}_2\text{O}_9$. Using the same estimate for $\langle S_i \cdot S_j \rangle$ and $\Delta\omega = -9.1 \text{ cm}^{-1}$, we find

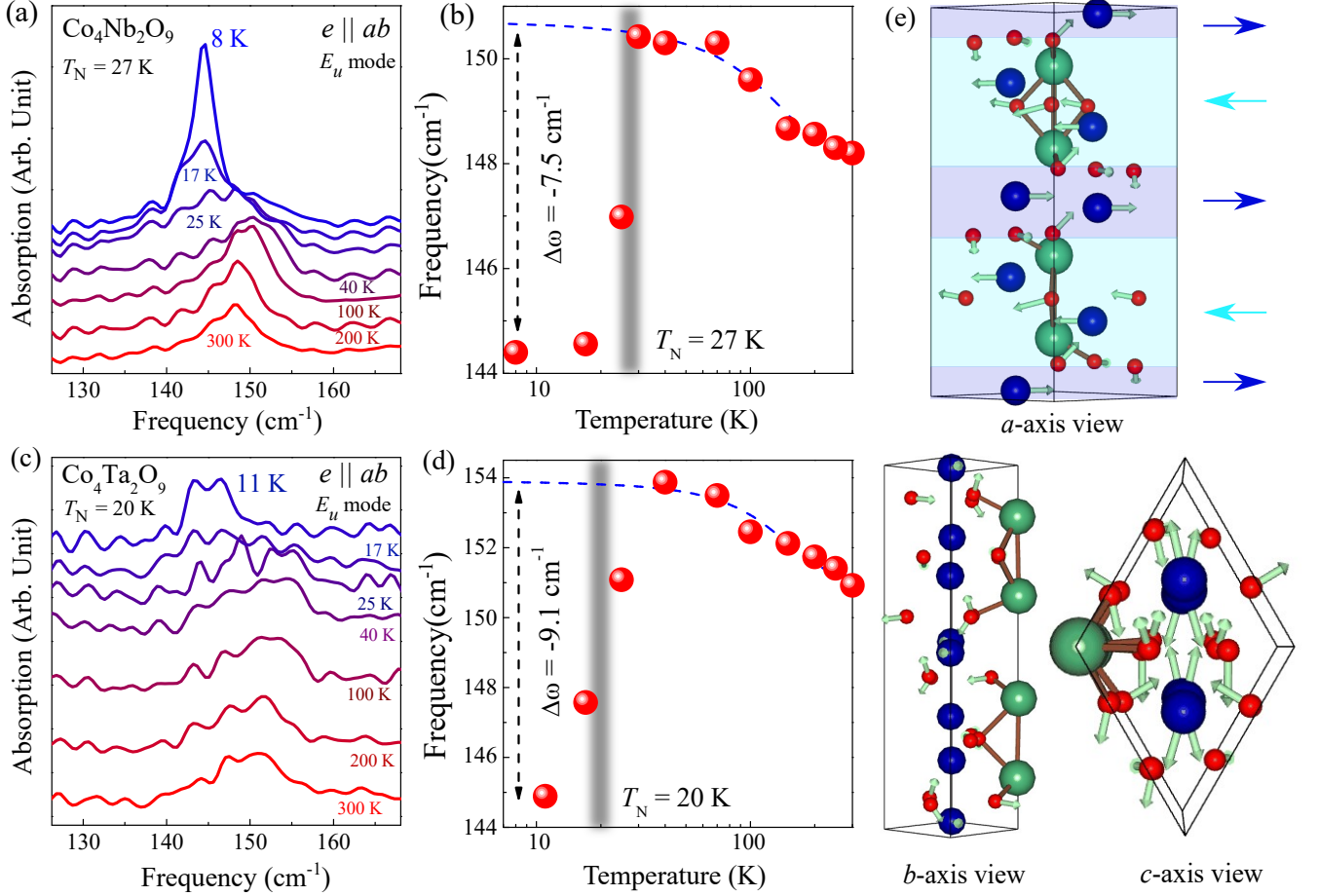


FIG. 2. (a, b) Absorption spectrum of $\text{Co}_4\text{Nb}_2\text{O}_9$ as a function of temperature and peak position vs. temperature for the 150 cm^{-1} shearing mode. (c, d) Similar results for $\text{Co}_4\text{Ta}_2\text{O}_9$. The spectra in (a, c) are shifted for clarity, and the blue dashed lines in (b, d) account for temperature effects. (e) Calculated displacement pattern of the E_u symmetry Co^{2+} layer shearing mode near 150 cm^{-1} .

$\lambda = -4.0\text{ cm}^{-1}$. This makes sense because Nb is a $4d$ element whereas Ta is $5d$, so the latter hosts more significant spin-orbit coupling.

We can extend this analysis to include additional effects. For instance, we can modify the spin-spin correlation function as $\langle S_i \cdot S_j \rangle \approx S^2 \cos^2(\Theta)$ in order to capture the noncollinearity of the spin states reported in our systems.^{25,26} This expression is a simple analog of Malus's rule for the polarization of light.⁵⁹ We use $\theta = 10.5^\circ$ and 14° to obtain $\lambda = -3.4$ and -4.3 cm^{-1} for $\text{Co}_4\text{Nb}_2\text{O}_9$ and $\text{Co}_4\text{Ta}_2\text{O}_9$, respectively.^{25,26} Accounting for non-collinearity increases spin-phonon coupling constants in the $\text{Co}_4\text{B}_2\text{O}_9$ materials by about 10%. These values are an order of magnitude larger than what was extracted for the aforementioned Raman-active modes,³³ so we see that coupling with odd- rather than even-symmetry vibrational modes is significantly more important.

We can also analyze the individual interactions between Co^{2+} sites. Here, it's important to recall that $\text{Co}_4\text{Nb}_2\text{O}_9$ and the Ta analog are composed of two different layers - akin to a superlattice consisting of planar

graphene and buckled SiC [Fig. 1(c, d)]. Writing down the spin Hamiltonian for the planar layer, the buckled layer, and the interaction terms between layers in a pairwise fashion, we obtain:

$$\hat{\mathcal{H}}_{spin} = \sum_{i,j} J_P S_i \cdot S_j + \sum_{i,j} J_B S_i \cdot S_j + \sum_{i,j} J_I S_i \cdot S_j. \quad (3)$$

Here, the J_P 's are in-plane exchange interactions, the J_B 's are those in the buckled layer, and the J_I 's couple the two layers quantifying interlayer exchange interactions. The S_i 's and S_j 's are the spins. Interestingly, both $\partial^2 J_P / \partial u_m \partial u_n$ and $\partial^2 J_B / \partial u_m \partial u_n$ are zero because the motion of interest does not modulate these exchange interactions [Section 4, Supplementary Information]. In other words, the in-plane terms can be ignored because the distances and angles do not change as a result of the displacement. Here, the $u_{n,m}$'s are the displacements (or distances) between Co centers. Writing down the force constant ($k_{n,m}$), we find that:

$$k_{n,m} = \frac{\partial^2 \hat{\mathcal{H}}_{spin}}{\partial u_m \partial u_n} = \frac{\partial^2 J_I}{\partial u_m \partial u_n} \langle S_i \cdot S_j \rangle = \lambda_I \langle S_i \cdot S_j \rangle. \quad (4)$$

TABLE I. Spin-phonon coupling in $\text{Co}_4\text{Nb}_2\text{O}_9$ and $\text{Co}_4\text{Ta}_2\text{O}_9$ compared with representative oxides. An asterisk (*) indicates estimated values.

Materials (cm^{-1})	Sites	Electronic state	ω_0 (cm^{-1})	$\Delta\omega$ (cm^{-1})	$\Delta\omega/\omega_0$ (cm^{-1})	λ (cm^{-1})	Refs.
ZnCr_2O_4	Cr^{3+}	$3d^3$	370	11	3%	6.2	15
CdCr_2O_4	Cr^{3+}	$3d^3$	365	9	2.5%	4	60
SrMnO_3	Mn^{4+}	$3d^3$	165	30*	18%*	4.8*	61
$\text{Fe}_{1-x}\text{Cu}_x\text{Cr}_2\text{S}_4$	Fe^{3+}	$3d^5$	120 to 400	-	<1.5 to 3%	-	62
Fe_2TeO_6	Fe^{3+}	$3d^5$	300 to 800	<1 to 5*	<1 to 1.3%*	0.1 to 1.2	63
Sr_2CoO_4	Co^{4+}	$3d^5$	630 and 410	-	-	2 to 3.5	64
MnF_2	Mn^{2+}	$3d^5$	≈ 56 to 480.5	2, -1.2, 2.7, 1.5*	≈ -0.4 to 3.7%*	0.4, 0.3, 0.3, -0.2	65
FeF_2	Fe^{2+}	$3d^6$	56 to 480.5	-	-	0.4, 0.3, -0.5, -1.3	65
$\text{Co}_4\text{Nb}_2\text{O}_9$	Co^{2+}	$3d^7$	144	-7.5	-5%	-3.4	This work
$\text{Co}_4\text{Ta}_2\text{O}_9$	Co^{2+}	$3d^7$	145	-9.1	-6%	-4.3	This work
NiO	Ni^{2+}	$3d^8$	752.5, 1160	-12.5, 25*	-1.7%*, -2.7%*	-7.9, 14.7	66
Ni_3TeO_6	Ni^{2+}	$3d^8$	313, 597.3, 672	-0.4, 0.3, -3.7	-0.1 to <1%*	-0.4, 0.3, -3.7	67
$\text{Y}_2\text{Ru}_2\text{O}_7$	Ru^{4+}	$4d^4$	420 and 492	-0.1 and -0.3	-0.2 and -0.6%*	-6 and -9	68
NaOsO_3	Os^{5+}	$5d^3$	550 to 800	40	$\approx 5.7\%*$	17.8*	69
$\text{Cd}_2\text{Os}_2\text{O}_7$	Os^{5+}	$5d^3$	100 to 800	-4.0 to 20*	-1 to 7%	-1.8 to 8.9 (with $S = 3/2$)*	69,70
$\text{Y}_2\text{Ir}_2\text{O}_7$	Ir^{4+}	$5d^4$	333, 425, 500	-0.8*, -1.6*, -6.5*	-0.2, -0.4, -1.3%	-0.4 to -3.2 (with $J_{\text{eff}} = 1/2$)*	71
$\text{Sr}_3\text{NiIrO}_6$	Ir^{4+}	$5d^4$	133, 310, 534	-	-	2, 10, 5	6
$\text{Ba}_2\text{FeReO}_6$	$\text{Fe}^{3+}/\text{Re}^{5+}$	$3d^5/5d^2$	390 to 630	≈ 30	5.1%*	-	72
$\text{Sr}_2\text{CrReO}_6$	$\text{Cr}^{3+}/\text{Re}^{5+}$	$3d^3/5d^2$	600	≈ 25	4.9%*	-	72

We therefore see that spin-phonon coupling in $\text{Co}_4\text{Nb}_2\text{O}_9$ and the Ta analog is entirely an inter-plane effect and that it is the Co shearing mode shown in Fig. 2(e) that modulates the interlayer magnetic interactions. It turns out that there are two primary types of inter-plane interactions in these systems. (We neglect the long interaction between Co centers along c because it is very small.) By analyzing the bond angles and their tendencies toward parallel or anti-parallel alignment based upon Goodenough-Kanamori-Anderson rules along with the number of near-neighbors, we can write:

$$\begin{aligned} \lambda_{\text{Total}} \langle S_i \cdot S_j \rangle &= \lambda_I \langle S_i \cdot S_j \rangle \\ &= \lambda_{2,FM} \langle S_i \cdot S_j \rangle + 3\lambda_{3,AFM} \langle S_i \cdot S_j \rangle. \end{aligned} \quad (5)$$

We immediately notice the competition between antiferromagnetic and ferromagnetic interlayer interactions in Eqn. 5 [and Fig. 1(d)], suggesting that $\text{Co}_4\text{Nb}_2\text{O}_9$ and $\text{Co}_4\text{Ta}_2\text{O}_9$ are frustrated. This competition reduces the overall size of the frequency shift across the magnetic ordering transition. It is also why the T_N 's are so low. We suspect that the magnitude of $\lambda_{2,FM}$ is larger than that of $\lambda_{3,AFM}$'s, but there are more $\lambda_{3,AFM}$'s in the sum leading to a slight preference for an antiferromagnetic ground state. The findings are consistent with softer O-Co-O bond angles and temperature-dependent lattice constants.^{27,33} As we discuss below, magnetoelectric coupling in these materials is likely to emanate from inter-layer spin-phonon interactions.

Table I summarizes the properties of several representative transition metal oxides, $4d$ - and $5d$ -containing systems, and $3d$ - $5d$ hybrids. The entries are grouped by the electronic state. We immediately notice that some

materials have multiple coupled modes and a tendency toward three-dimensional structure whereas others have only a single spin-phonon coupled mode along with a tendency toward layered or chain-like character. As already discussed, the E_u symmetry Co^{2+} shearing mode near 150 cm^{-1} is the only feature to engage in spin-phonon coupling in the materials of interest here. We also see that the frequency shifts in Table I have both positive and negative signs. Among the materials with coupled modes that soften, $\text{Co}_4\text{Nb}_2\text{O}_9$ and the Ta analog host the largest relative frequency shift - even though competing antiferromagnetic and ferromagnetic interactions reduce the size of the overall shift.

The spin-phonon coupling constant, λ , is often challenging to define, and the procedure for doing so is inconsistent in the literature. We therefore find the relative frequency shifts to be the most reliable for comparison purposes. As pointed out in Ref. 70, the relative frequency shift of a phonon across a magnetic ordering transition $\Delta\omega/\omega_0$ is usually less than 1% for a transition metal oxide. $\text{Co}_4\text{Nb}_2\text{O}_9$ and the Ta analog are different with relative frequency shifts of -5 and -6%, respectively. These values are unusually large. In fact, the $\Delta\omega/\omega_0$'s that we find in $\text{Co}_4\text{Nb}_2\text{O}_9$ and $\text{Co}_4\text{Ta}_2\text{O}_9$ [Fig. 2(b, d)] are more comparable with the $5d$ oxides and $3d/5d$ hybrid systems shown in Table I where the relative frequency shifts correlate (in general) with the electronic shell and spin-orbit coupling.

The presence of a heavy element at the B site in $\text{Co}_4\text{Nb}_2\text{O}_9$ and $\text{Co}_4\text{Ta}_2\text{O}_9$ naturally raises questions about the spin Hamiltonian and whether additional terms such as anisotropy and Dzyaloshinskii-Moriya interactions contribute to spin-phonon coupling.^{14,68,71,73} Recent neutron scattering also demonstrates that the excitation spectrum can not be reproduced without

terms that give rise to spin noncollinearity.^{24,25} Focusing on $\text{Co}_4\text{Nb}_2\text{O}_9$, we see that the anisotropies $\geq J$'s \geq Dzyaloshinskii-Moriya interaction.^{24,25} All of these terms are on the order of 1 meV. Of course, we are not interested in the absolute size of the anisotropy, exchange, or Dzyaloshinskii-Moriya interaction. Instead, we want to know how they are modulated by the 150 cm^{-1} phonon mode. In other words, we are interested in how these quantities *change* with respect to the displacement. By using the mode symmetry and details of the displacement pattern, we can identify the terms that are important for spin-phonon coupling as well as those that will likely cancel out.

If we modify Eqn. 4 to include these terms, the prefactors that contribute to spin-phonon coupling are $\partial^2 A/\partial u^2$ and $\partial^2 DM/\partial u^2$. Here A is the anisotropy, and DM is the Dzyaloshinskii-Moriya interaction. The question is whether these contributions are large or small. Since A is an on-site term, we do not expect it to change very much with a vibration. Even if it does, we anticipate that shearing of the planar vs. buckled layers against each other will significantly diminish $\partial^2 A/\partial u^2$ due to their opposite motion. In other words, while $\partial^2 A/\partial u^2$ for the planar and buckled layers are not exactly equal, they have opposite signs due to the shearing motion of the layers which, when added together, diminish any impact of the overall anisotropy term. Therefore, we argue that in these unique circumstances $\partial^2 A/\partial u^2$ is small. On the other hand, the $\partial^2 DM/\partial u^2$ term multiplies a cross product between two sites and has the potential to contribute. However, spin-orbit coupling and noncollinearity derive primarily from the B site, suggesting reduced importance because the displacement pattern does not involve the movement of the B site. Another way to consider the issue is that the Dzyaloshinskii-Moriya interaction is in the Co-O-Co linkage of the buckled layers, and these bond lengths and angles do not change with the motion.²⁴ This again rules out contributions from the Dzyaloshinskii-Moriya interaction.

Magnetoelectric coupling in the Co_4B_2O_9 ($B = \text{Nb}, \text{Ta}$) family of materials has been of sustained interest.^{23,30,35,36} Suggested mechanisms include spin-phonon coupling,^{28,29} domain and domain wall effects,³⁰ Dzyaloshinskii-Moriya interactions through the spin-current model,^{24,38} and critical spin fluctuations.^{27,30} With the direct observation of large frequency shifts across the magnetic ordering transitions, sizeable spin-phonon coupling constants, and microscopic analysis of the competing interlayer interactions, we are in a better position to evaluate how magnetoelectric coupling might emerge from these candidate mechanisms. As established above, our analysis reveals that $\text{Co}_4\text{Nb}_2\text{O}_9$ and the Ta analog have strong spin-phonon interactions that involve competing interlayer exchange interactions modulated by the shearing motion of the Co layers. While there are Raman-active modes that are sensitive to the development of magnetic ordering,³³ the infrared-active E_u symmetry Co^{2+} layer shearing mode has a fre-

quency shift that is an order of magnitude larger, indicating that odd-symmetry motion dominates spin-phonon coupling in this system. This type of exchange striction provides a very natural origin for magnetodielectric coupling.^{23,28,29,38} It is also the most likely origin of magnetoelectric coupling^{23,28,29} given the fact that the Dzyaloshinskii-Moriya interaction operating through the spin-current model is significantly smaller and does not couple to the Co^{2+} layer shearing mode near 150 cm^{-1} . The change in dipole moment associated with magnetoelectric coupling⁷⁴ is consistent with the microscopic nature of this infrared-active mode.

To summarize, we measured the vibrational properties of $\text{Co}_4\text{Nb}_2\text{O}_9$ and the Ta analog and compared our findings with lattice dynamics calculations and a detailed model of spin-phonon coupling. In addition to revealing one of the largest relative frequency shifts ever reported, these materials host a Co shearing mode that couples only with the interlayer interactions due to unique symmetry conditions. These interlayer interactions are frustrated. Given the sizable contribution of spin-phonon interactions in these systems, it is likely that magnetoelectric coupling is driven by this effect.

SUPPLEMENTARY INFORMATION

See Supplementary information for the complete description of the vibrational modes, displacement patterns, the temperature dependence of phonons, spin-phonon analysis, and phonon lifetimes as a function of temperature.

Research at the University of Tennessee is supported by the U.S. Department of Energy, Office of Basic Energy Sciences, Materials Science Division under award DE-FG02-01ER45885. SWC was supported by the center for Quantum Materials Synthesis (cQMS), funded by the Gordon and Betty Moore Foundation's EPiQS initiative through GBMF10104 and by Rutgers University. D.V. was supported by the NSF (DMR-1954856). V.K. was supported by the National Science Foundation (DMR-2103625). S.C. was supported by the Institute for Basic Science (IBS-R011-Y3). D. G. Oh, N. Lee, and Y. J. Choi were supported by the National Research Foundation of Korea (NRF-2017R1A5A1014862 (SRC program: vdWMRC center), NRF-2019R1A2C2002601, and NRF-2021R1A2C1006375). J.H.L. at UNIST was supported by Midcareer Researcher (2020R1A2C2103126) and Creative Materials Discovery (2017M3D1A1040828) programs through the National Research Foundation of Korea.

I. AUTHOR DECLARATIONS

Conflict of Interest

The authors have no conflicts to disclose.

Author Contributions

KP and JLM designed the study. CK, DGO, NL, SWC, and YJC grew the crystals. KP performed the variable temperature measurements. KP and JLM analyzed the spectral data. JK and DV performed DFT calculations. KP, JK, SC, SF, VK, and JLM discussed the measurement results and analysis in detail. KP, JHL, and JLM developed a spin Hamiltonian model. KP, JK, and JLM wrote the manuscript. All authors read and commented on the text.

DATA AVAILABILITY

The data that support the findings of this study are available from the corresponding author upon reasonable request.

REFERENCES

- ¹A. E. Taylor, S. Calder, R. Morrow, H. L. Feng, M. H. Upton, M. D. Lumsden, K. Yamaura, P. M. Woodward, and A. D. Christianson, *Phys. Rev. Lett.* **118**, 207202 (2017).
- ²B. Zwartsenberg, R. P. Day, E. Razzoli, M. Michiardi, N. Xu, M. Shi, J. D. Denlinger, G. Cao, S. Calder, K. Ueda, J. Bertinshaw, H. Takagi, B. J. Kim, I. S. Elfimov, and A. Damascelli, *Nature Physics* **16**, 290 (2020).
- ³H.-H. Kim, K. Ueda, S. Nakata, P. Wochner, A. Mackenzie, C. Hicks, G. Khaliullin, H. Liu, B. Keimer, and M. Minola, *Nature Communications* **13**, 6674 (2022).
- ⁴S. Varotto, A. Johansson, B. Göbel, L. M. Vicente-Arche, S. Mallik, J. Bréhin, R. Salazar, F. Bertran, P. L. Fèvre, N. Bergeal, J. Rault, I. Mertig, and M. Bibes, *Nature Communications* **13**, 6165 (2022).
- ⁵J. Singleton, J. W. Kim, C. V. Topping, A. Hansen, E.-D. Mun, S. Chikara, I. Lakis, S. Ghannadzadeh, P. Goddard, X. Luo, Y. S. Oh, S.-W. Cheong, and V. S. Zapf, *Phys. Rev. B* **94**, 224408 (2016).
- ⁶K. R. O’Neal, A. Paul, A. Al-Wahish, K. D. Hughey, A. L. Blockmon, X. Luo, S.-W. Cheong, V. S. Zapf, C. V. Topping, J. Singleton, M. Ozerov, T. Birol, and J. L. Musfeldt, *npj Quantum Mater.* **4**, 48 (2019).
- ⁷S. Bordács, D. Varjas, I. Kézsmárki, G. Mihály, L. Baldassarre, A. Abouelsayed, C. A. Kuntscher, K. Ohgushi, and Y. Tokura, *Phys. Rev. Lett.* **103**, 077205 (2009).
- ⁸C. Kant, J. Deisenhofer, T. Rudolf, F. Mayr, F. Schrettle, A. Loidl, V. Gnezdilov, D. Wulferding, P. Lemmens, and V. Tsurkan, *Phys. Rev. B* **80**, 214417 (2009).
- ⁹A. L. Wysocki and T. Birol, *Phys. Rev. B* **93**, 134425 (2016).
- ¹⁰R. Morrow, R. Mishra, O. D. Restrepo, M. R. Ball, W. Windl, S. Wurmehl, U. Stockert, B. Büchner, and P. M. Woodward, *J. Am. Chem. Soc.* **135**, 18824 (2013).
- ¹¹B. Yan, A. K. Paul, S. Kanungo, M. Reehuis, A. Hoser, D. M. Többens, W. Schnelle, R. C. Williams, T. Lancaster, F. Xiao, J. S. Möller, S. J. Blundell, W. Hayes, C. Felser, and M. Jansen, *Phys. Rev. Lett.* **112**, 147202 (2014).
- ¹²R. Datta, S. K. Pradhan, S. Masanta, S. Majumdar, and S. K. De, *J. Solid State Chem.* **314**, 123391 (2022).
- ¹³C. Martins, M. Aichhorn, and S. Biermann, *J. Phys. Condens. Matter* **29**, 263001 (2017).
- ¹⁴T. Kim, C. H. Kim, J. Jeong, P. Park, K. Park, K. H. Lee, J. C. Leiner, D. Ishikawa, A. Q. R. Baron, Z. Hiroi, and J.-G. Park, *Phys. Rev. B* **102**, 201101 (2020).
- ¹⁵A. B. Sushkov, O. Tchernyshyov, W. R. II, S. W. Cheong, and H. D. Drew, *Phys. Rev. Lett.* **94**, 137202 (2005).
- ¹⁶C. J. Fennie and K. M. Rabe, *Phys. Rev. Lett.* **96**, 205505 (2006).
- ¹⁷J. H. Lee, L. Fang, E. Vlahos, X. Ke, Y. W. Jung, L. F. Kourkoutis, J.-W. Kim, P. J. Ryan, T. Heeg, M. Roeckerath, V. Goian, M. Bernhagen, R. Uecker, P. C. Hammel, K. M. Rabe, S. Kamba, J. Schubert, J. W. Freeland, D. A. Muller, C. J. Fennie, P. Schiffer, V. Gopalan, E. Johnston-Halperin, and D. G. Schlom, *Nature* **466**, 954 (2010).
- ¹⁸M. Mochizuki, N. Furukawa, and N. Nagaosa, *Phys. Rev. B* **84**, 144409 (2011).
- ¹⁹N. A. Spaldin and R. Ramesh, *Nature Materials* **18**, 203 (2019).
- ²⁰E. Bertaut, L. Corliss, F. Forrat, R. Aleonard, and R. Pauthenet, *J. Phys. Chem. Solids* **21**, 234 (1961).
- ²¹T. Kolodiaznyy, H. Sakurai, and N. Vittayakorn, *Appl. Phys. Lett.* **99**, 132906 (2011).
- ²²Y. Cao, Y. Yang, M. Xiang, Z. Feng, B. Kang, J. Zhang, W. Ren, and S. Cao, *J. Cryst. Growth* **420**, 90 (2015).
- ²³N. D. Khanh, N. Abe, H. Sagayama, A. Nakao, T. Hanashima, R. Kiyonagi, Y. Tokunaga, and T. Arima, *Phys. Rev. B* **93**, 075117 (2016).
- ²⁴G. Deng, Y. Cao, W. Ren, S. Cao, A. J. Studer, N. Gauthier, M. Kenzelmann, G. Davidson, K. C. Rule, J. S. Gardner, P. Imperia, C. Ulrich, and G. J. McIntyre, *Phys. Rev. B* **97**, 085154 (2018).
- ²⁵L. Ding, M. Lee, T. Hong, Z. Dun, R. Sinclair, S. Chi, H. K. Agrawal, E. S. Choi, B. C. Chakoumakos, H. Zhou, and H. Cao, *Phys. Rev. B* **102**, 174443 (2020).
- ²⁶S. Choi, D. G. Oh, M. J. Gutmann, S. Pan, G. Kim, K. Son, J. Kim, N. Lee, S.-W. Cheong, Y. J. Choi, and V. Kiryukhin, *Phys. Rev. B* **102**, 214404 (2020).
- ²⁷L. H. Yin, Y. M. Zou, J. Yang, J. M. Dai, W. H. Song, X. B. Zhu, and Y. P. Sun, *Appl. Phys. Lett.* **109**, 032905 (2016).
- ²⁸Y. M. Xie, C. S. Lin, H. Zhang, and W. D. Cheng, *AIP Adv.* **6**, 045006 (2016).
- ²⁹N. D. Khanh, N. Abe, K. Matsuura, H. Sagayama, Y. Tokunaga, and T. Arima, *Appl. Phys. Lett.* **114**, 102905 (2019).
- ³⁰Y. Fang, S. Yan, L. Zhang, Z. Han, B. Qian, D. Wang, and Y. Du, *J. Am. Ceram. Soc.* **98**, 2005 (2015).
- ³¹Y. Fang, Y. Q. Song, W. P. Zhou, R. Zhao, R. J. Tang, H. Yang, L. Y. Lv, S. G. Yang, D. H. Wang, and Y. W. Du, *Sci. Rep.* **4**, 3860 (2015).
- ³²L. Zhou, H. Song, K. Liu, Z. Luan, P. Wang, L. Sun, S. Jiang, H. Xiang, Y. Chen, J. Du, H. Ding, K. Xia, J. Xiao, and D. Wu, *Science Advances* **4** (2018), 10.1126/sciadv.aao3318.
- ³³S. Yadav, M. Chandra, R. Rawat, A. Khandelwal, L. S. Chandra, R. J. Choudhary, V. Sathe, A. Sinha, and K. Singh, *J. Phys. Chem. C* **126**, 14986 (2022).
- ³⁴R. Dagar, S. Yadav, M. Kinha, B. S. Mehra, R. Rawat, K. Singh, and D. S. Rana, *Phys. Rev. Mater.* **6**, 074409 (2022).
- ³⁵Y. Cao, G. Deng, P. Beran, Z. Feng, B. Kang, J. Zhang, N. Guiblin, B. Dkhil, W. Ren, and S. Cao, *Sci. Rep.* **7**, 14079 (2017).
- ³⁶N. Lee, D. G. Oh, S. Choi, J. Y. Moon, J. H. Kim, H. J. Shin, K. Son, J. Nuss, V. Kiryukhin, and Y. J. Choi, *Sci. Rep.* **10**, 12362 (2020).
- ³⁷Y. M. Xie, H. Zang, W. D. Ceng, H. Y. Wu, and C. C. Wang, *Applied Physics Letters* **113**, 082906 (2018).
- ³⁸I. V. Solovyev and T. V. Kolodiaznyy, *Phys. Rev. B* **94**, 094427 (2016).

- ³⁹M. Matsumoto and M. Koga, *J. Phys. Soc. Jpn.* **88**, 094704 (2019).
- ⁴⁰K. Chakarawet, M. Atanasov, J. E. Ellis, W. W. Lukens, V. G. Young, R. Chatterjee, F. Neese, and J. R. Long, *Inorg. Chem.* **60**, 18553 (2021).
- ⁴¹F. Wooten, *Optical Properties of Solids* (Elsevier, 1972).
- ⁴²G. Kresse and J. Furthmüller, *Phys. Rev. B* **54**, 11169 (1996).
- ⁴³G. Kresse and J. Furthmüller, *Comput. Mater. Sci.* **6**, 15 (1996).
- ⁴⁴P. E. Blöchl, *Phys. Rev. B* **50**, 17953 (1994).
- ⁴⁵G. Kresse and D. Joubert, *Phys. Rev. B* **59**, 1758 (1999).
- ⁴⁶J. P. Perdew, K. Burke, and M. Ernzerhof, *Phys. Rev. Lett.* **77**, 3865 (1996).
- ⁴⁷S. L. Dudarev, G. A. Botton, S. Y. Savrasov, C. J. Humphreys, and A. P. Sutton, *Phys. Rev. B* **57**, 1505 (1998).
- ⁴⁸M. Gajdoš, K. Hummer, G. Kresse, J. Furthmüller, and F. Bechstedt, *Phys. Rev. B* **73**, 045112 (2006).
- ⁴⁹A. Togo and I. Tanaka, *Scr. Mater.* **108**, 1 (2015).
- ⁵⁰X. Gonze and C. Lee, *Phys. Rev. B* **55**, 10355 (1997).
- ⁵¹T. R. Paudel and W. R. L. Lambrecht, *Phys. Rev. B* **76**, 115205 (2007).
- ⁵²K. D. Hughey, A. J. Clune, M. O. Yokosuk, A. al Wahish, K. R. O’Neal, S. Fan, N. Abhyankar, H. Xiang, Z. Li, J. Singleton, N. S. Dalal, and J. L. Musfeldt, *Phys. Rev. B* **96**, 180305 (2017).
- ⁵³S. Fan, S. Neal, C. Won, J. Kim, D. Sapkota, F. Huang, J. Yang, D. G. Mandrus, S.-W. Cheong, J. T. Haraldsen, and J. L. Musfeldt, *Nano Lett.* **21**, 99 (2021).
- ⁵⁴Q. C. Sun, D. Mazumdar, L. Yadgarov, R. Rosentsveig, R. Tenne, and J. L. Musfeldt, *Nano Letters* **13**, 2803 (2013).
- ⁵⁵A. Lughini and S. Sanvito, *Science Advances* **5**, eaax7163 (2019).
- ⁵⁶E. Granado, A. García, J. A. Sanjurjo, C. Rettori, I. Torriani, F. Prado, R. D. Sánchez, A. Caneiro, and S. B. Oseroff, *Phys. Rev. B* **60**, 11879 (1999).
- ⁵⁷T. Birol and C. J. Fennie, *Phys. Rev. B* **88**, 094103 (2013).
- ⁵⁸W. Baltensperger, *J. Appl. Phys.* **41**, 1052 (1970).
- ⁵⁹E. Collett, *Field guide to polarization* (SPIE, 2005).
- ⁶⁰R. Valdés-Aguilar, A. B. Sushkov, Y. J. Choi, S.-W. Cheong, and H. D. Drew, *Phys. Rev. B* **77**, 092412 (2008).
- ⁶¹S. Kamba, V. Goian, V. Skoromets, J. Hejtmánek, V. Bovtun, M. Kempa, F. Borodavka, P. Vaněk, A. A. Belik, J. H. Lee, O. Pacherová, and K. M. Rabe, *Phys. Rev. B* **89**, 064308 (2014).
- ⁶²T. Rudolf, K. Pucher, F. Mayr, D. Samusi, V. Tsurkan, R. Tidecks, J. Deisenhofer, and A. Loidl, *Phys. Rev. B* **72**, 014450 (2005).
- ⁶³P. Pal, S. Badola, P. Biswas, R. R. Das, S. Saha, S. Kaushik, P. Rajput, P. Vishwakarma, and A. Singh, *J. Magn. Magn. Mater.* **540**, 168512 (2021).
- ⁶⁴P. K. Pandey, R. J. Choudhary, D. K. Mishra, V. G. Sathe, and D. M. Phase, *Appl. Phys. Lett.* **102**, 142401 (2013).
- ⁶⁵D. J. Lockwood and M. G. Cottam, *J. Appl. Phys.* **64**, 5876 (1988).
- ⁶⁶E. Aytan, B. Debnath, F. Kargar, Y. Barlas, M. M. Lacerda, J. X. Li, R. K. Lake, J. Shi, and A. A. Balandin, *Appl. Phys. Lett.* **111**, 252402 (2017).
- ⁶⁷M. O. Yokosuk, S. Artyukhin, A. al Wahish, X. Wang, J. Yang, Z. Li, S.-W. Cheong, D. Vanderbilt, and J. L. Musfeldt, *Phys. Rev. B* **92**, 144305 (2015).
- ⁶⁸J. S. Lee, T. W. Noh, J. S. Bae, I.-S. Yang, T. Takeda, and R. Kanno, *Phys. Rev. B* **69**, 214428 (2004).
- ⁶⁹S. Calder, J. H. Lee, M. B. Stone, M. D. Lumsden, J. C. Lang, M. Feyngenson, Z. Zhao, J.-Q. Yan, Y. G. Shi, Y. S. Sun, Y. Tsujimoto, K. Yamaura, and A. D. Christianson, *Nat Commun.* **6**, 8916 (2015).
- ⁷⁰C. H. Sohn, C. H. Kim, L. J. Sandilands, N. T. M. Hien, S. Y. Kim, H. J. Park, K. W. Kim, S. J. Moon, J. Yamaura, Z. Hiroi, and T. W. Noh, *Phys. Rev. Lett.* **118**, 117201 (2017).
- ⁷¹J. Son, B. C. Park, C. H. Kim, H. Cho, S. Y. Kim, L. J. Sandilands, C. Sohn, J.-G. Park, S. J. Moon, and T. W. Noh, *npj Quantum Mater.* **4**, 17 (2019).
- ⁷²A. F. García-Flores, A. F. L. Moreira, U. F. Kaneko, F. M. Ardito, H. Terashita, M. T. D. Orlando, J. Gopalakrishnan, K. Ramesha, and E. Granado, *Phys. Rev. Lett.* **108**, 177202 (2012).
- ⁷³H. J. Silverstein, K. Fritsch, F. Flicker, A. M. Hallas, J. S. Gardner, Y. Qiu, G. Ehlers, A. T. Savici, Z. Yamani, K. A. Ross, B. D. Gaulin, M. J. P. Gingras, J. A. M. Paddison, K. Foyevtsova, R. Valenti, F. Hawthorne, C. R. Wiebe, and H. D. Zhou, *Phys. Rev. B* **89**, 054433 (2014).
- ⁷⁴N. A. Spaldin, *J. Exp. Theor. Phys.* **132**, 493 (2021).